Electronic Supplementary Material (ESI) for Journal of Materials Chemistry A.

Supporting Information

Tailoring Carrier Dynamics in Inverted Mesoporous Perovskite Solar Cells with Interface-Engineered Plasmonics

Zhiliang Liu, Qingcheng Li, Kun Chen, Yuying Cui, Jeremy J. Intemann, Shifeng Leng, Minghuan Cui, Chaochao Qin, Linfeng Fei, Kai Yao and Haitao Huang

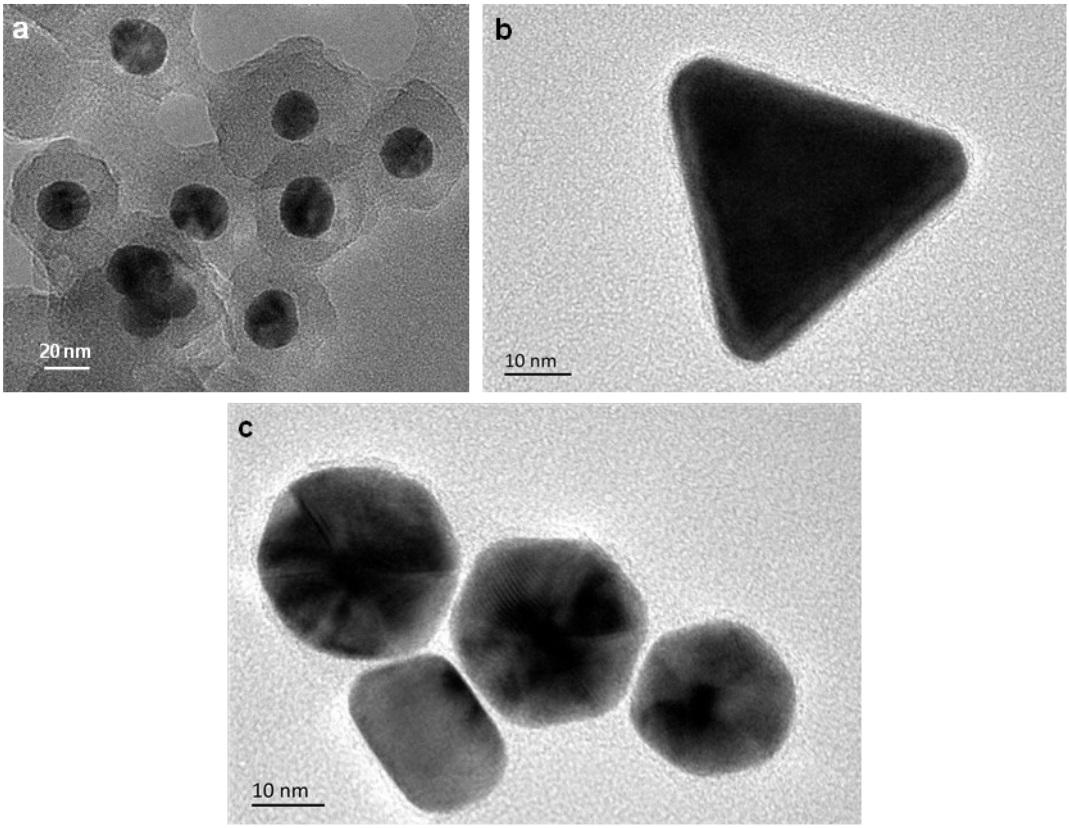

Fig. S1. (a) TEM micrographs of Au-nanospheres@NiO_x with shell thickness of ~15 nm. (b) TEM micrographs of Au-nanoprism@NiO_x with shell thickness of ~3 nm. (c) TEM micrographs of Au-nanosphere@NiO_x with shell thickness of ~3 nm.

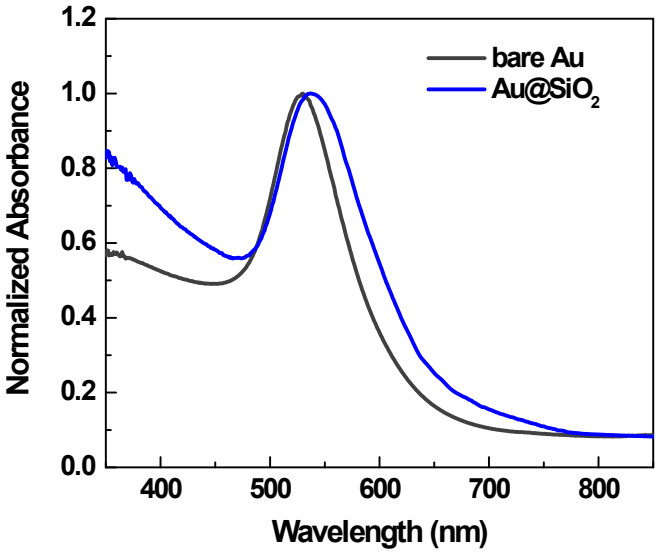

Fig. S2. UV-vis spectra of bare Au as well as $Au@SiO_2$ NPs in ethanol.

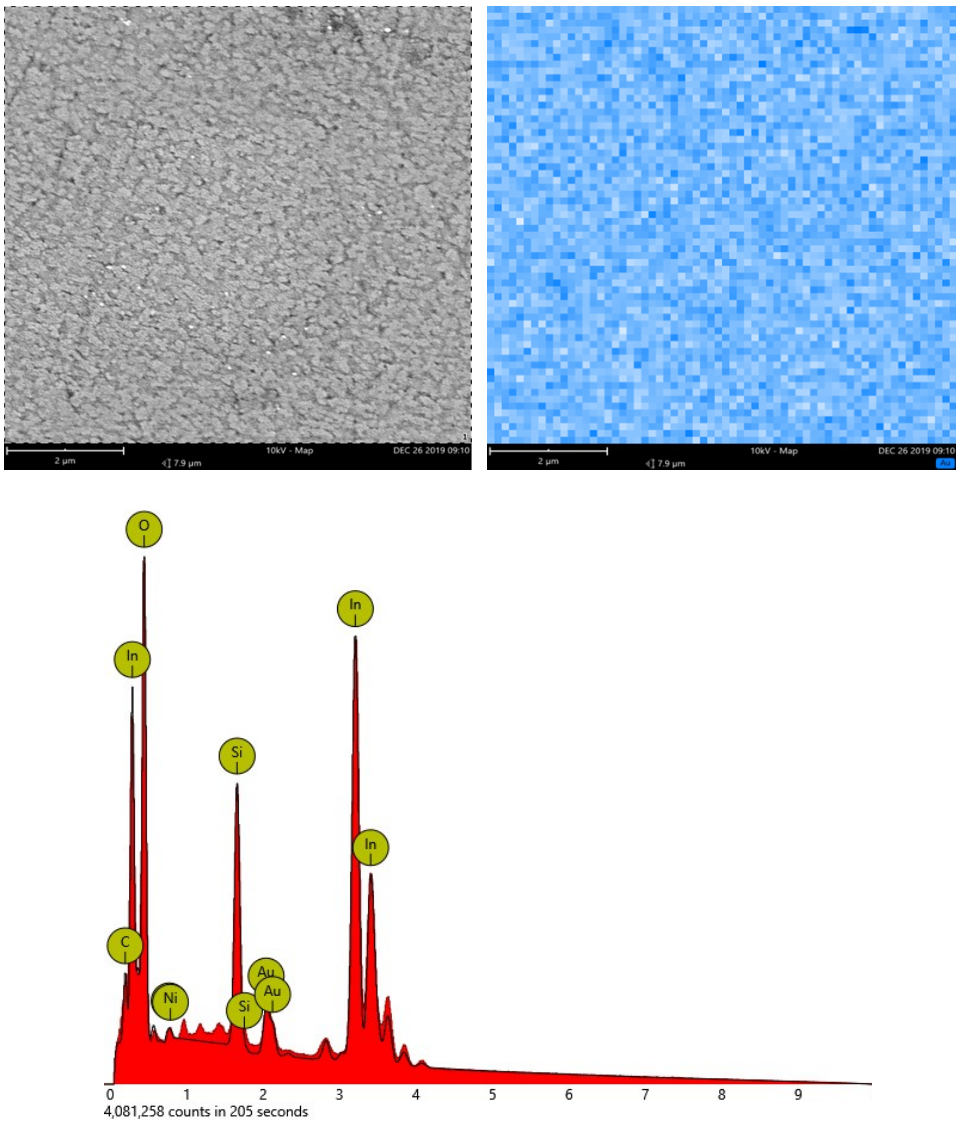

Fig. S3. Top view SEM image of mp-NiO_x film doped with $Au@NiO_x$ NPs and EDX mapping results of the same region.

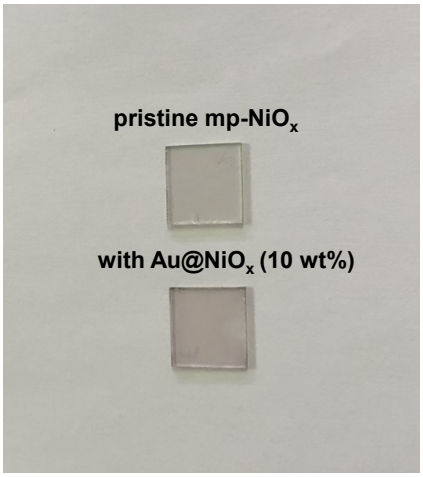

Fig. S4. The photographs of the mp-NiO_x films cast on quartz glass with or without Au@NiO_x NPs (10 wt%).

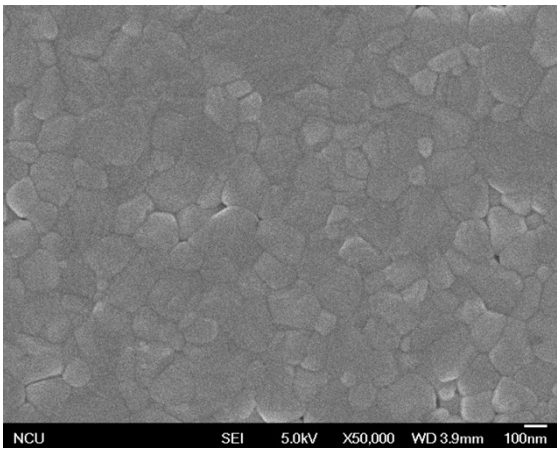

Fig. S5. Top view SEM images of the CsFA perovskite films on mp-NiO_x films with Au@SiO_2 (5 wt%) incorporation.

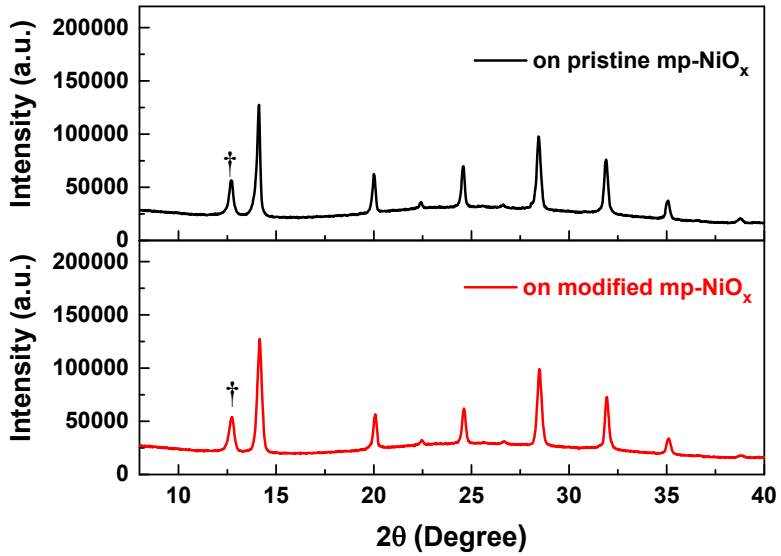

Fig. S6. X-ray diffraction patterns of CsFA perovskite films on pristine mp-NiO_x and Au@NiO_x embedded mp-NiO_x films. The labeled signal is corresponding to the residual PbI_2.

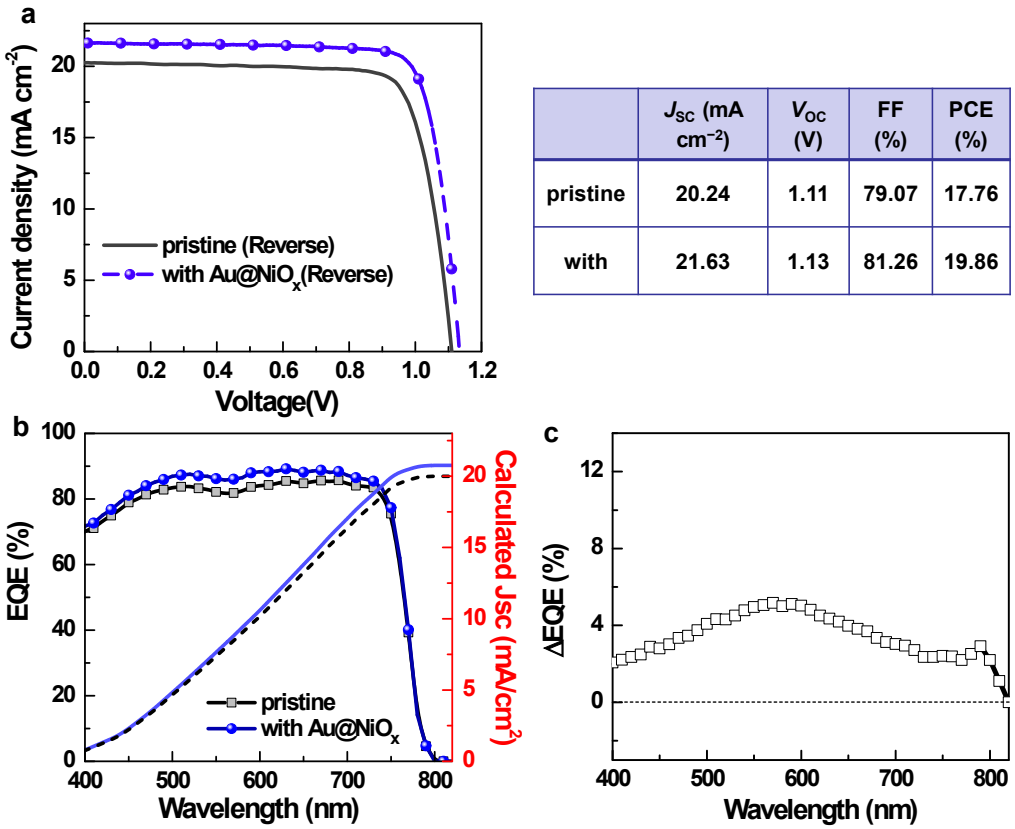

	J_{SC} (mA cm^{-2})	V_{OC} (V)	FF (%)	PCE (%)
pristine	20.24	1.11	79.07	17.76
with	21.63	1.13	81.26	19.86

Fig. S7. (a) *J–V* curves of the champion PSCs prepared with the pristine and Au@NiOx containing mp-NiO_x layer measured with backward scans. The right table shows the performance of mesoporous PSCs without surface treatment. (b) Wavelength-dependent EQE and integrated J_{SC} curve for the pristine and Au@NiO_x embedded PSCs. (c) Enhanced EQE ratio of device caused by the Au@NiO_x NPs incorporation.

Table S1. Performance of champion CsFA device based on mp-NiO_x without and with incorporation of plasmonic NPs.

Materials	Scan Direction	J_{SC} (mA cm^{-2})	V_{OC} (V)	FF (%)	PCE (%)	hysteresis index (HI)[a]
pristine	Forward	20.32	1.12	77.07	17.54	0.026
pristine	Reverse	20.40	1.12	79.72	18.21	
with Au@SiO_2	Forward	20.87	1.12	76.15	17.80	0.034
with Au@SiO_2	Reverse	20.86	1.12	79.28	18.52	
with Au@NiO_x	Forward	21.80	1.15	81.06	20.32	0.011
with Au@NiO_x	Reverse	21.75	1.15	82.42	20.61	

[a)]The definition of hysteresis index (HI) value is [HI = 1– $J_{FS}(0.8V_{OC})/J_{RS}(0.8V_{OC})$], where $J_{RS}(0.8V_{OC})$ and $J_{FS}(0.8V_{OC})$ stand for photocurrent density at 80% of V_{OC} for the reverse and forward sweep, respectively.

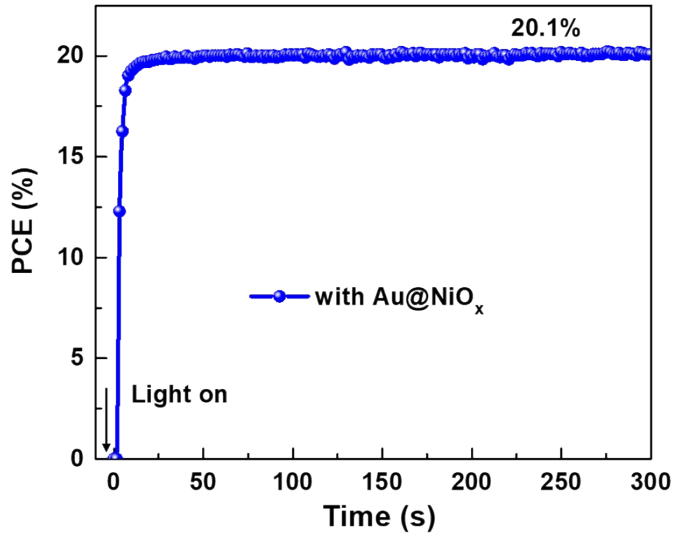

Fig. S8. Stabilized PCEs at maximum power point output of the champion PSC prepared on Au@NiO_x containing mp-NiO_x layer.

Table S2. Summary of MA-free mesoporous PSCs with high efficiencies under simulated solar light condition (AM 1.5).

Perovskite Materials	Device Structure	J_{SC} (mA cm^{-2})	V_{OC} (V)	FF	PCE (%)[a]	PCE (%)[b]
$Rb_{0.05}FA_{0.95}PbI_3$ (bandgap 1.53 eV)	FTO/bl-TiO_2/mp-TiO_2/ perovskite/ Spiro-OMeTAD/Au	23.93	1.07	0.67	17.2[1]	16.8
$Cs_{0.20}FA_{0.80}PbI_3$-(Cl) (bandgap 1.56 eV)	FTO/bl-TiO_2/mp-TiO_2/ perovskite/ Spiro-OMeTAD/Au	24.10	1.10	0.78	20.6[2]	19.9
$(Cs_{0.17}FA_{0.83})Pb(I_{0.89}Br_{0.08}Cl_{0.03})_3$ (bandgap 1.58 eV)	FTO/bl-TiO_2/mp-TiO_2/SnO_2/ perovskite/Spiro-OMeTAD/Au	23.28	1.12	0.78	20.5[3]	–
$(CsPbBr_3)_{0.06}(FAPbI_3)_{0.94}$ (bandgap 1.55 eV)	FTO/bl-TiO_2/mp-TiO_2/ perovskite/ Spiro-OMeTAD/Au	24.52	1.15	0.78	21.8[4]	21.1
$(Cs_{0.15}FA_{0.85})Pb(I_{0.9}Br_{0.1})_3$ (bandgap ~1.58 eV)	FTO/bl-NiO_x/mp-$CuGaO_2$/ perovskite/$PC_{61}BM$/BCP/Ag	23.19	1.11	0.80	20.7[5]	20.2
$(Cs_{0.17}FA_{0.83})Pb(I_{0.8}Br_{0.2})_3$ (bandgap 1.61 eV)	FTO/bl-NiO_x/mp-NiO_x/ perovskite/bFPI/$PC_{61}BM$/BCP/Ag	21.75	1.15	0.82	20.6 (this work)	20.1

[a)]Measured from J-V curve;
[b)]measured from steady-state power output;
[c)]The bandgap values are quoted from references and some values are not explicitly stated. In such case, we extracted the optical bandgap values from corresponding absorption spectra.

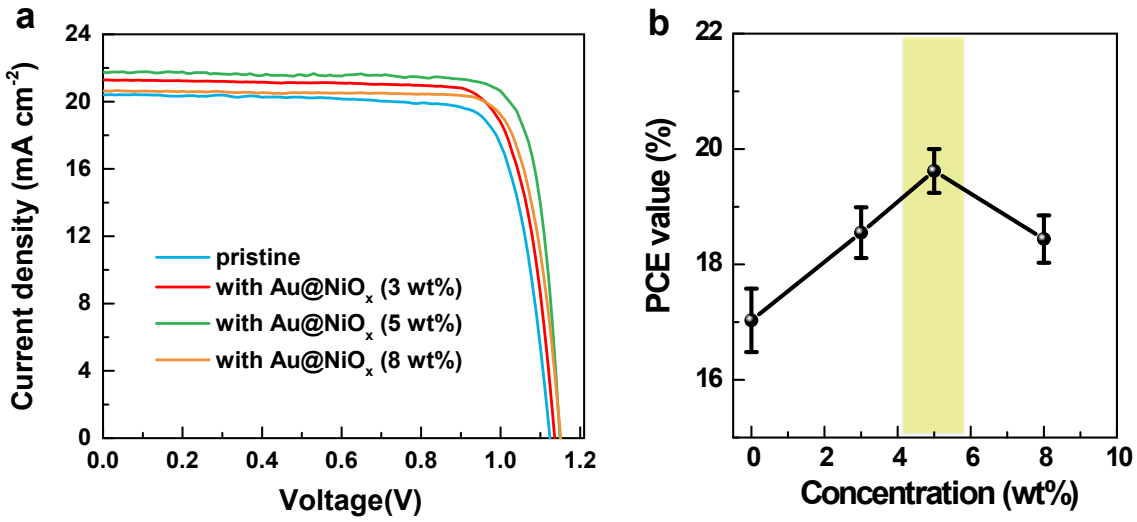

Fig. S9. (a) *J–V* characteristics for inverted mesoporous solar cells with increasing Au@NiO_x concentration (0 ≤ Au@NiO_x ≤ 8 wt%). (b) Variations in PCE valule of CsFA devices as a function of the doping concentration of Au@NiO_x in mp-NiO_x layer.

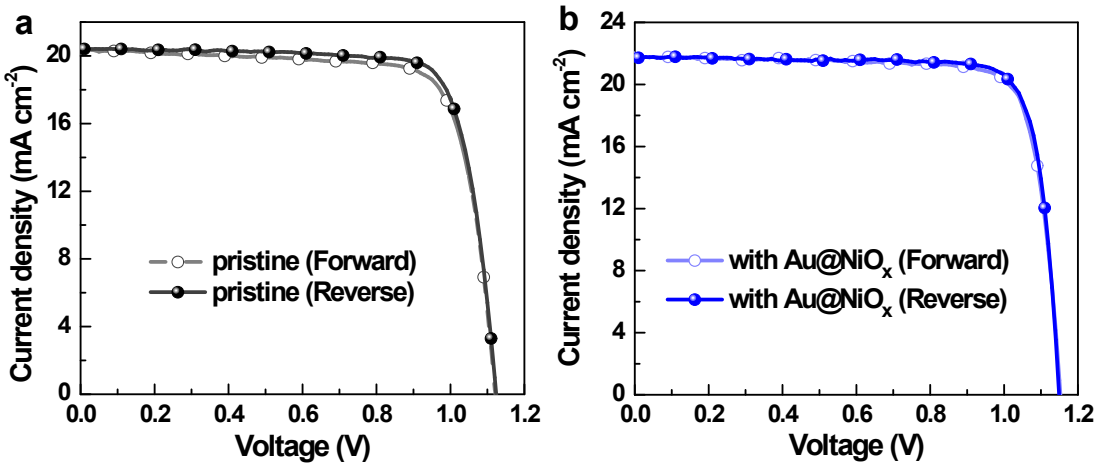

Fig. S10. The *J*-*V* curve from the reverse scan (from *V*oc to *J*sc) and forward scan (from *J*sc to *V*oc) for the champion (a) pristine and (b) Au@NiO_x-modified devices under 1 Sun condition.

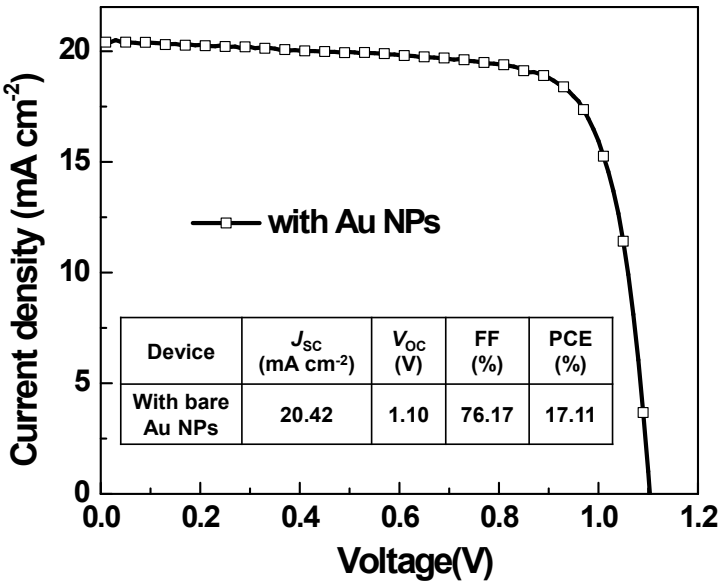

Fig. S11. *J*–*V* curves of the control PSC device fabricated on bare Au containing mp-NiO_x. The inset show the photovaltics parametars.

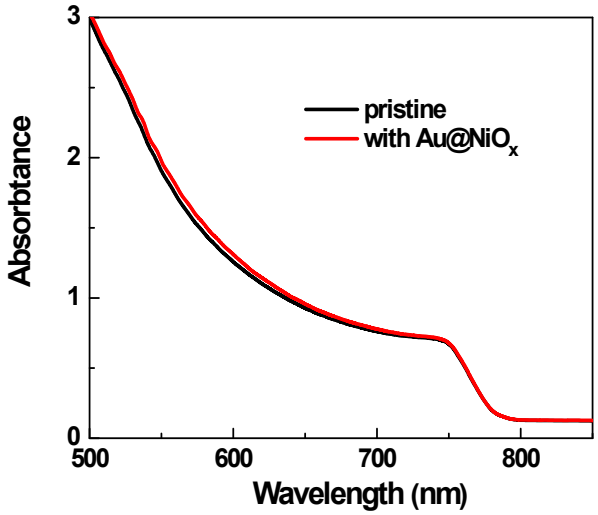

Fig. S12. UV–vis spectra (obtained with an integrating sphere) of CsFA perovskite films deposited on mp-NiO_x films without and with Au@NiO_x (5 wt%) incorporation.

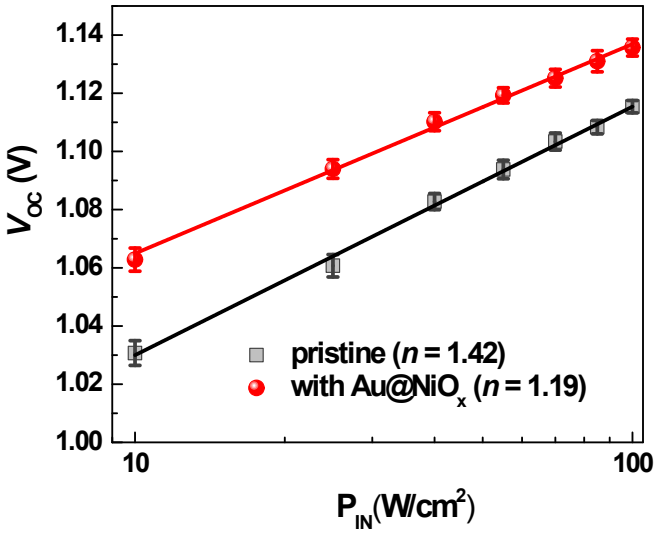

Fig. S13. V_{OC} versus light intensity for the CsFA PSCs without and with Au@NiOx incorporation. A natural logarithmic relationship between V_{OC} and light intensity yields a slope of $n = \frac{q}{kTd\ln(\varphi)}\frac{dV_{OC}}{}$, where n is the ideality factor, k is the Boltzmann's constant, T is the temperature, and q is an elementary charge, according to the Shockley–Read–Hall theory.

Table S3. The electrical properties of mp-NiO_x film extracted from Hall effect measurement measurements and four-probe measurement.

mp-NiO_x film	hole conductivity σ_p (Ω cm^{-2})[a]	hole concentration p (cm^{-3})[b]	hole mobility μ_p ($cm^2/V{\cdot}s$)[c]
pristine	3.2×10^{-4}	3.9×10^{17}	5.1×10^{-3}
with Au@NiO_x	7.7×10^{-3}	5.4×10^{18}	8.9×10^{-3}
with Au@SiO_2	5.2×10^{-4}	6.1×10^{17}	5.3×10^{-3}

[a)]Measured from four-probe measurement; [b)]Measured from Hall effect measurement;

[c]Obtained by derivation of equation $\sigma_p = pq\mu_p$.

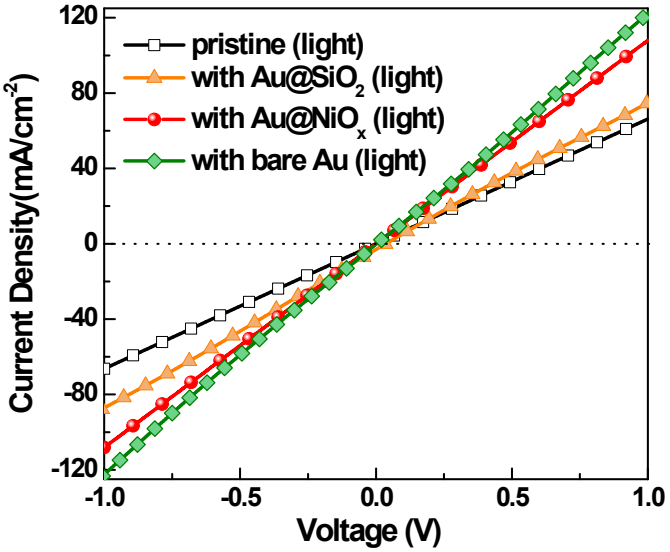

Fig. S14. *J-V* characteristics for conductivity test of pristine, Au-doped, Au@SiO_2-doped and Au@NiO_x-doped mp-NiO_x films obtained by linear sweep voltammetry under simulated sunlight (AM1.5).

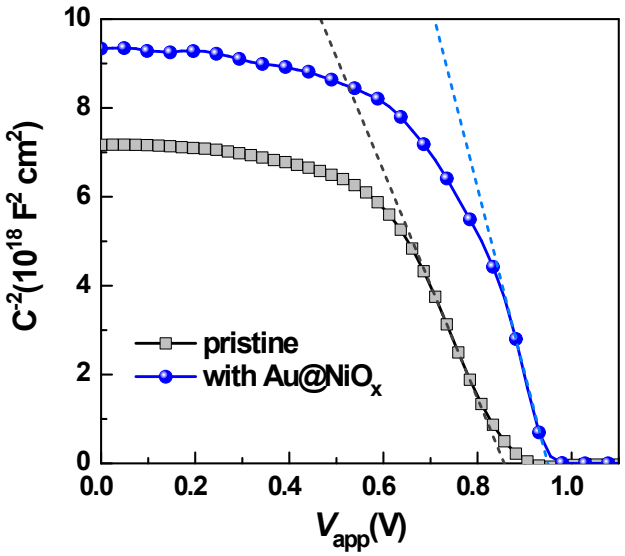

Fig. S15. Capacitance-voltage curve plotted according to Mott–Schottky relation for pristine and Au@NiO_x containing devices at 1 kHz. These plots directly demonstrate the higher flat-band potential of the modified device compared with the pristine device, which is related to an increase in V_{OC}.

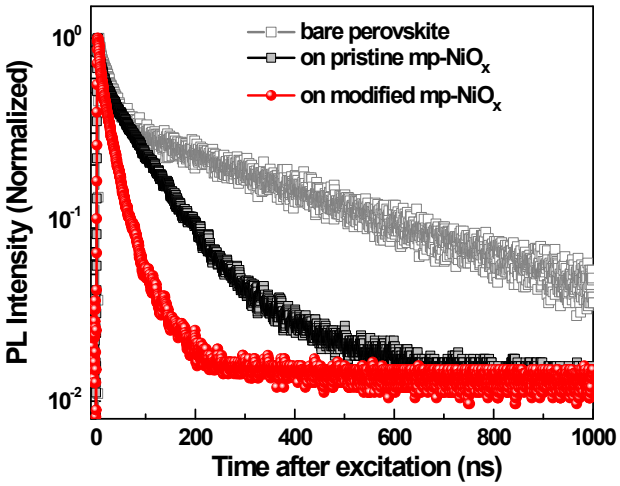

Fig. S16. Time-resolved PL spectra (probed at 775 nm) of CsFA perovskite deposited on quartz glass, pristine mp-NiO_x film and Au@NiO_x containing mp-NiO_x film.

Table S4. Time resolved photoluminescence characterization of the perovskite films on various substrates.

Sample	τ_1 (ns)	Fraction 1	τ_2 (ns)	Fraction 2	Average (ns)
on glass	23.9	42.7%	438.6	57.3%	261.4
on pristine mp-NiO_x	6.5	82.1%	95.6	17.9%	22.4
on Au@NiO_x containing mp-NiO_x	4.1	89.7%	34.8	10.3%	7.3

Note: The decay is fitted with bimolecular model: $I(t) = I_0 + A_1 \exp\left(-t/\tau_1\right) + A_2 exp(-t/\tau_2)$, ($\tau_1$ and τ_2 give the fast and slow decay time constant, A_1 and A_2 are fractions of the decay processes.

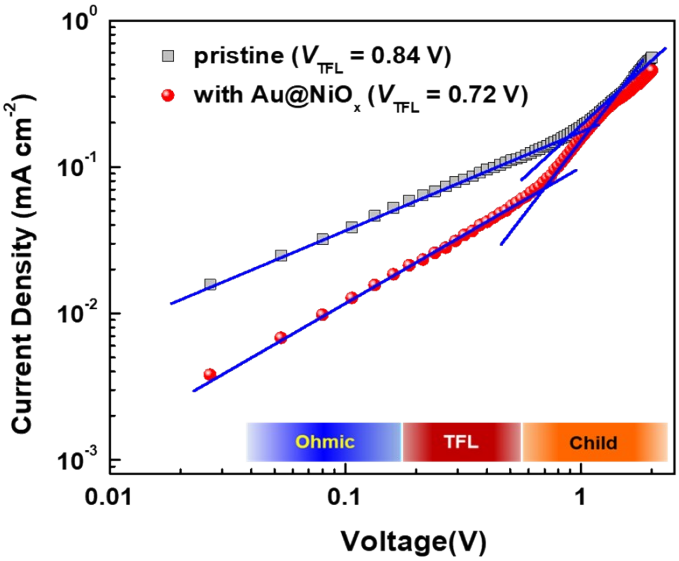

Fig. S17. Dark *J–V* of the hole-only devices without and with Au@NiO_x modification as determined by the space-charge-limited current (SCLC) method, displaying V_{TFL} kink point. The trap density N_{trap} is determined by the equation: $V_{TFL} = eN_{trap}L^2/(2\varepsilon\varepsilon_0)$, where V_{TFL} is trap-filled limit voltage, L is the thickness of CsFA film, ε is the relative dielectric constant of perovskite, and ε_0 is the vacuum permittivity.

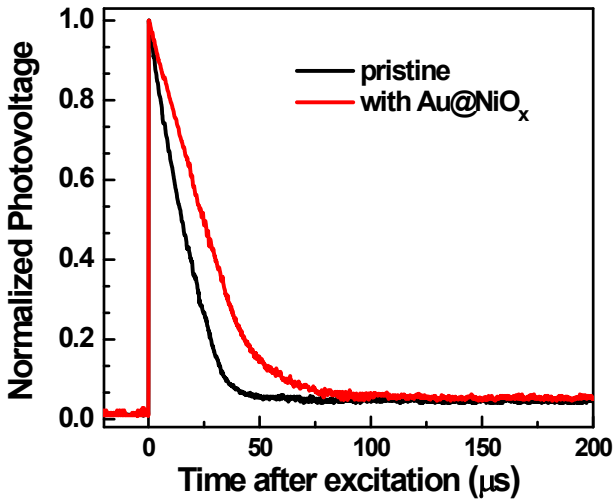

Fig. S18. TPV decay curve under white bias light with intensity equivalent to 0.1-Sun (10 mW cm^{-2}) generated by white light source with small voltage perturbation (532 nm).

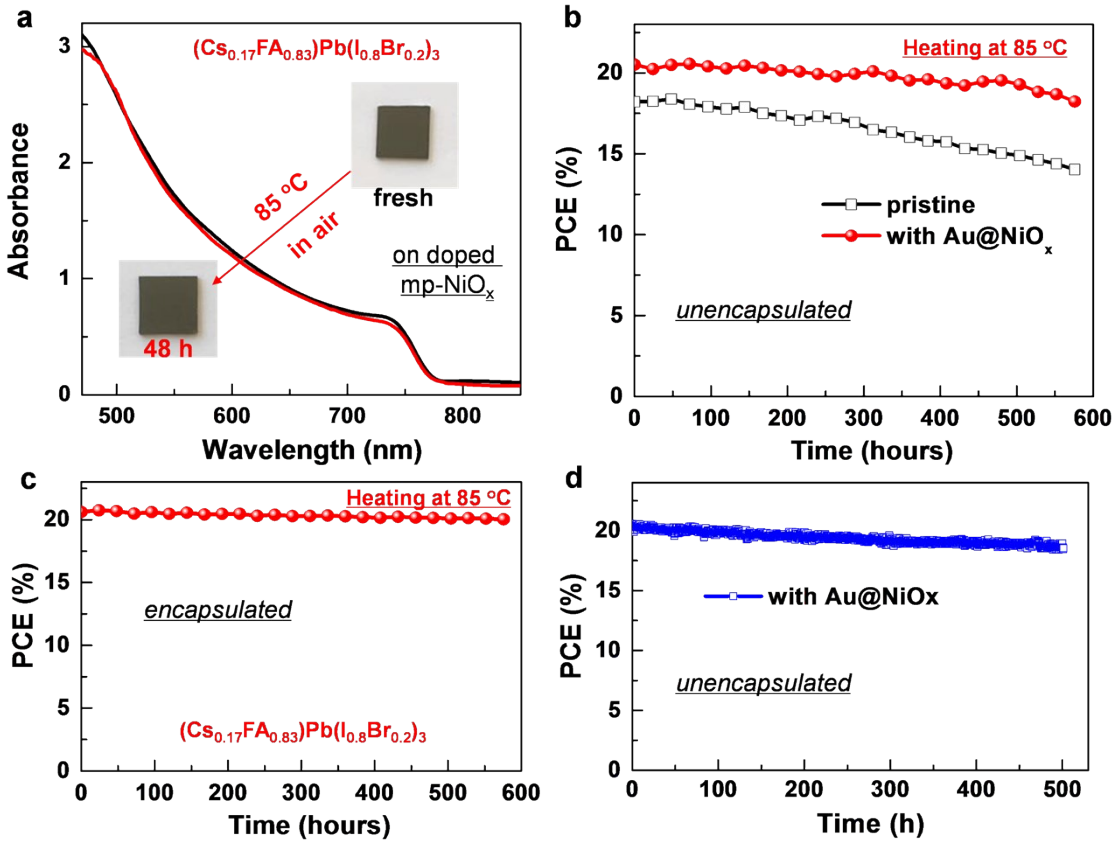

Fig. S19. Stability evaluation. (a) UV-visible absorption of $(Cs_{0.17}FA_{0.83})Pb(I_{0.8}Br_{0.2})_3$ (CsFA) perovskite film on Au@NiOx-doped mp-NiOx scaffold before and after annealing in air at 85 °C for 48 hours under ambient condition with 50–70% RH. The insets show the corresponding optical images. (b) Thermal aging testing of unencapsulated devices without and with modification. (c) Aging testing of encapsulated devices heated continuously at 85 °C tracked by PCE measurement at periodic intervals for 12 h. (d) Operational stability measurement of the unencapsulated devices based on Au@NiOx-modified PSCs under continuous 1-sun illumination at ambient condition with 50–70% RH.

Supporting References

1. Y. H. Park, I. Jeong, S. Bae, H. J. Son, P. Lee, J. Lee, C.-H. Lee and M. J. Ko, *Adv. Funct. Mater.*, 2017, **27**, 1605988.

2. D. Prochowicz, R. Runjhun, M. M. Tavakoli, P. Yadav, M. Saski, A. Q. Alanazi, D. J. Kubicki, Z. Kaszkur, S. M. Zakeeruddin, J. Lewiński and M. Grätzel, *Chem. Mater.*, 2019, **31**, 1620-1627.

3. X. X. Gao, W. Luo, Y. Zhang, R. Hu, B. Zhang, A. Zuttel, Y. Feng and M. K. Nazeeruddin, *Adv. Mater.*, 2020, **32**, 1905502.

4. L. Xie, K. Lin, J. Lu, W. Feng, P. Song, C. Yan, K. Liu, L. Shen, C. Tian and Z. Wei, *J. Am. Chem. Soc.*, 2019, **141**, 20537-20546.

5. Y. Chen, Z. Yang, X. Jia, Y. Wu, N. Yuan, J. Ding, W.-H. Zhang and S. Liu, *Nano Energy*, 2019, **61**, 148-157.